THE ASTRONOMICAL JOURNAL, 122:1697–1706, 2001 October

THE SUBPARSEC-SCALE STRUCTURE AND EVOLUTION OF CENTAURUS A. II. CONTINUED VERY LONG BASELINE ARRAY MONITORING

S. J. TINGAY
Paul Wild Observatory, CSIRO Australia Telescope National Facility, Locked Bag 194, Narrabri, NSW 2390, Australia; stingay@atnf.csiro.au
R. A. PRESTON
Jet Propulsion Laboratory, California Institute of Technology, Mail Stop 238-332, 4800 Oak Grove Drive, Pasadena, CA 91109
AND
D. L. JAUNCEY
CSIRO Australia Telescope National Facility, P.O. Box 76, Epping, NSW 2121, Australia
Received 2001 May 7; accepted 2001 June 20

ABSTRACT

We present the results of continued 8.4 GHz Very Long Baseline Array monitoring of the subparsec-scale structure and evolution of Centaurus A, following on from the initial results presented in 1998 by Tingay et al. We include, for the first time, multiepoch VLBI images at 22.2 GHz that show that the jet is linear and well collimated on scales as small as 0.02 pc ($\sim 1000 r_s$). Two components in the subparsec-scale jet continue to evolve slowly with a speed of $0.12c$. We confirm that an additional component, close to the core, has no significant motion. Some evidence is seen for rapid variations within individual components, as noted dramatically in 1991–1992 by Tingay et al., albeit at a lower level of activity. Both the stationary behavior of the component close to the core and the internal variability of components in the subparsec-scale jet of Centaurus A may be explained as being due to the existence of shocks created in the wake of major component ejections from the nucleus, as simulated by Agudo et al. (published in 2001). Tentative evidence is found to suggest that two subparsec-scale counterjet components are in motion away from the nucleus. The estimated apparent speeds of the jet and counterjet components are consistent with the previously suggested likely jet viewing angle range, 50°–80°. We also compare our Centaurus A images with high-resolution VLBI images of M87 to show that the region of the Centaurus A jet in which collimation likely first occurs lies a factor of 10 below our current resolution limit. Future space VLBI missions at high frequency will be required to resolve this region.

Key words: galaxies: active — galaxies: individual (NGC 5128, Centaurus A, PKS 1322−427) — radio continuum — techniques: interferometric

1. INTRODUCTION

Centaurus A (PKS 1322−427, NGC 5128) is the closest classical radio galaxy, at a distance of approximately 3.4 Mpc (Israel 1998). In comparison, the well-studied nearby radio galaxy M87 lies at a distance of 14.7 Mpc (Jacoby, Ciardullo, & Ford 1990), 4 times more distant than Centaurus A. Previous investigations of the large- and small-scale radio properties of Centaurus A have been summarized by Tingay et al. (1998, hereafter T98), who presented an 8 yr sequence of VLBI images at 2.3, 4.8, 8.4, and 22.2 GHz, from both the Very Long Baseline Array (VLBA) and the Southern Hemisphere VLBI Experiment (SHEVE). This series of images shows that the subparsec-scale structure of Centaurus A is complex, consisting of a bright jet and a fainter counterjet. Components in the jet appear to have a gradual motion away from the nucleus of approximately $0.1c$, while episodes of rapid internal evolution in one particular component (C1) led T98 to suggest that the underlying flow of the jet is much faster, greater than $0.45c$. Considering the likely jet speed and the jet-to-counterjet surface brightness ratio (Jones et al. 1996), T98 conclude that the jet is inclined to our line of sight by between 50° and 80°.

Recently, Tingay & Murphy (2001) have presented multifrequency VLBA observations of the subparsec-scale jet in Centaurus A to investigate the effects of free-free absorption along the line of sight to the galaxy nucleus; they measure an inverted nuclear spectral index between 2.2 and 5.0 GHz of $3.8 \pm {}^{0.6}_{0.5}$ and estimate that the free-free optical depth toward the nucleus is 0.9 ± 0.4 at a frequency of 2.2 GHz.

Also recently, advances have been made in other regions of the photon spectrum that yield information on the nuclear environment. Kraft et al. (2000) have published high-resolution X-ray images of Centaurus A from *Chandra* data that show the relationship between the X-ray and radio emission of the jet on kiloparsec scales. Infrared observations have been used to detect a 20 pc disk of material at the center of the galaxy (Schreier et al. 1998), and Marconi et al. (2001) have estimated the mass of the central black hole in Centaurus A to be $2.0 \pm {}^{3.0}_{1.4} \times 10^8 M_\odot$, from infrared spectra obtained at the Very Large Telescope (VLT).

By virtue of its proximity, Centaurus A is clearly one of the most important targets of study in the quest to gain an understanding of the jet formation and collimation mechanisms in AGNs. Thus, in this paper, we present the results of continued VLBA monitoring of Centaurus A at frequencies of 8.4 and 22.2 GHz over the period 1997–2000. This period of continued monitoring allows us to confirm the apparent speeds of components C1 and C2 and to determine that the component C3 has a much smaller apparent speed than C1 or C2. C3 may be a quasi-stationary extension to the nucleus, as similarly seen in other high spatial resolution images of radio jets (Tingay et al. 1995; Gómez et al. 2000).

We have also tentatively detected the motions of counterjet components on the subparsec-scale that may eventually

TABLE 1

PARAMETERS OF THE VLBI MAPS

Epoch (1)	Frequency (GHz) (2)	Figure (3)	Map Size (pixels) (4)	Cell Size (mas) (5)	Peak (Jy beam^{-1}) (6)	Noise (mJy beam^{-1}) (7)	S_{total} (Jy) (8)	Beam Position Angle (mas) (9)	Position Angle (deg) (10)
1997 Jan 23....	8.4	1*a*	512	0.5	2.0	6	5.6	3.1 × 15.5	10.6
1997 Jan 23....	22.2	1*b*	512	0.25	1.5	8	2.7	1.2 × 5.6	10.5
1997 Mar 24...	8.4	1*c*	512	0.5	1.7	3	5.2	3.3 × 15.0	7.3
1997 Mar 24...	22.2	1*d*	512	0.25	1.9	5	3.3	1.2 × 5.0	6.4
1997 Jul 20	8.4	1*e*	512	0.5	1.9	4	4.7	3.0 × 13.6	12.0
1997 Jul 20	22.2	1*f*	512	0.25	0.9	6	1.4	1.1 × 5.8	12.3
1998 Apr 14 ...	8.4	1*g*	512	0.5	1.4	7	5.2	2.3 × 9.0	−4.5
1998 Aug 8	8.4	1*h*	512	0.5	2.1	2	5.5	3.1 × 11.5	9.2
1998 Dec 19 ...	8.4	1*i*	512	0.5	2.0	2	5.5	3.8 × 15.0	−9.4
1999 May 1....	8.4	1*j*	512	0.5	1.9	8	4.5	3.1 × 12.4	8.6
2000 Jan 15....	8.4	1*k*	512	0.5	1.2	3	4.2	2.1 × 10.9	−5.8

NOTES.—Col. (1): the observation date; col. (2): the observation frequency; col. (3): the figure number; col. (4): the map size in pixels; col. (5): cell size in milliarcseconds; col. (6): the peak flux density in the map in janskys per beam; col. (7): the off-source rms noise level in the map in millijanskys per beam; col. (8): the total flux density in the map in janskys; col. (9): the restoring beam position angle FWHM dimensions in milliarcseconds; col. (10): position angles in degrees.

lead to strong constraints on the true component speeds and the jet viewing angle.

In § 2, we describe our VLBA observations. In § 3, we present the results of the recent observations in conjunction with the results of T98, bringing the overall time base of Centaurus A VLBI monitoring to over 11 yr. In § 4, we discuss the nature of the stationary component C3, tentative constraints on the true component speed and jet angle to the line of sight, and compare the jet collimation region scales in Centaurus A and M87.

2. DATA REDUCTION AND ANALYSIS

Table 1 lists our VLBA observations over the period 1997–2000. At epochs where both 8.4 and 22.2 GHz data were obtained, we switched between the two frequencies on a 22 minute timescale.

All the observations used the VLBA recording format and were made with an aggregate bit rate of 128 Mb s^{-1}, a 1 bit sampling, and a 64 MHz band broken into eight intermediate frequencies. All data were correlated at the VLBA processor in Socorro, New Mexico. The correlated data were read into AIPS, amplitude-calibrated, and fringe-fitted using the method recommended in the AIPS cookbook. If both 8.4 and 22.2 GHz data were present in the same observation, the two frequencies were split immediately after they were read into AIPS, before any major processing.

We made an attempt to correct the 22 GHz data for atmospheric opacity effects in AIPS, using the task APCAL to calculate corrections via both the grid search and minimization options. In both cases, the corrections appeared to improve the data somewhat, but it seems that significant errors remain, probably due to the fact that the opacity corrections are difficult to model for Centaurus A, which at a declination of almost −44° is observed at low elevations at most of the VLBA antennas. The final data reduction includes opacity corrections using the simple grid search option in the AIPS task APCAL.

Once fringe-fitted and averaged in frequency, the data were exported into the DIFMAP software (Shepherd, Pearson, & Taylor 1994) for editing and imaging. Specifically, all data to the Mauna Kea and Saint Croix antennas were flagged, since they represent outlier stations; the baselines involving these antennas contain valuable high-resolution information but produce large holes in the *u-v* plane that seriously degrade the images. The remaining array (excluding the Brewster and Hancock antennas, since they are too far north) has been used. For imaging, initially phase-only self-calibration was used in conjunction with a tight clean window on the brightest region of the source. In subsequent clean–self-calibrate iterations, the clean windows were extended to include fainter emission, although only the phases were self calibrated. Finally, when the flux density of the clean model reached the level of the amplitudes on the shorter baselines, amplitude self-calibration was performed initially with a timescale much longer than the observation length and subsequently on shorter timescales. The maps resulting from the imaging procedure are shown in temporal order in Figure 1.

3. RESULTS

3.1. *8.4 GHz Data*

A montage of the 8.4 GHz images is shown in Figure 2. The solid lines superposed on Figure 2 are discussed below. The subparsec-scale structure and evolution of the series of 8.4 GHz images over the period 1997–2000 has been investigated by fitting sets of model components to the *u-v* plane data, as was done for the earlier data of T98. However, whereas T98 used the Caltech VLBI package task MODELFIT (Pearson 1991) to undertake model fitting, for the current data, we have used the DIFMAP software (Shepherd et al. 1994) to undertake model fitting. Tests of MODELFIT and DIFMAP on the same data sets show a high degree of consistency between the results, and DIFMAP has the added advantage of being able to model-fit in conjunction with hybrid imaging. Other than this change in the software used, the model fitting of the 1997–2000 data and the estimates of errors on the model parameters proceeded as described in T98. Table 2 gives the model-fit parameters for each of the 8.4 GHz data sets obtained between 1997 and 2000. In each model, only Gaussian components have been used.

Figure 3 (equivalent to Figs. 3 and 5 in T98) shows the apparent motions of the components C1, C2, and C3 relative to the (presumed stationary) core component as a func-

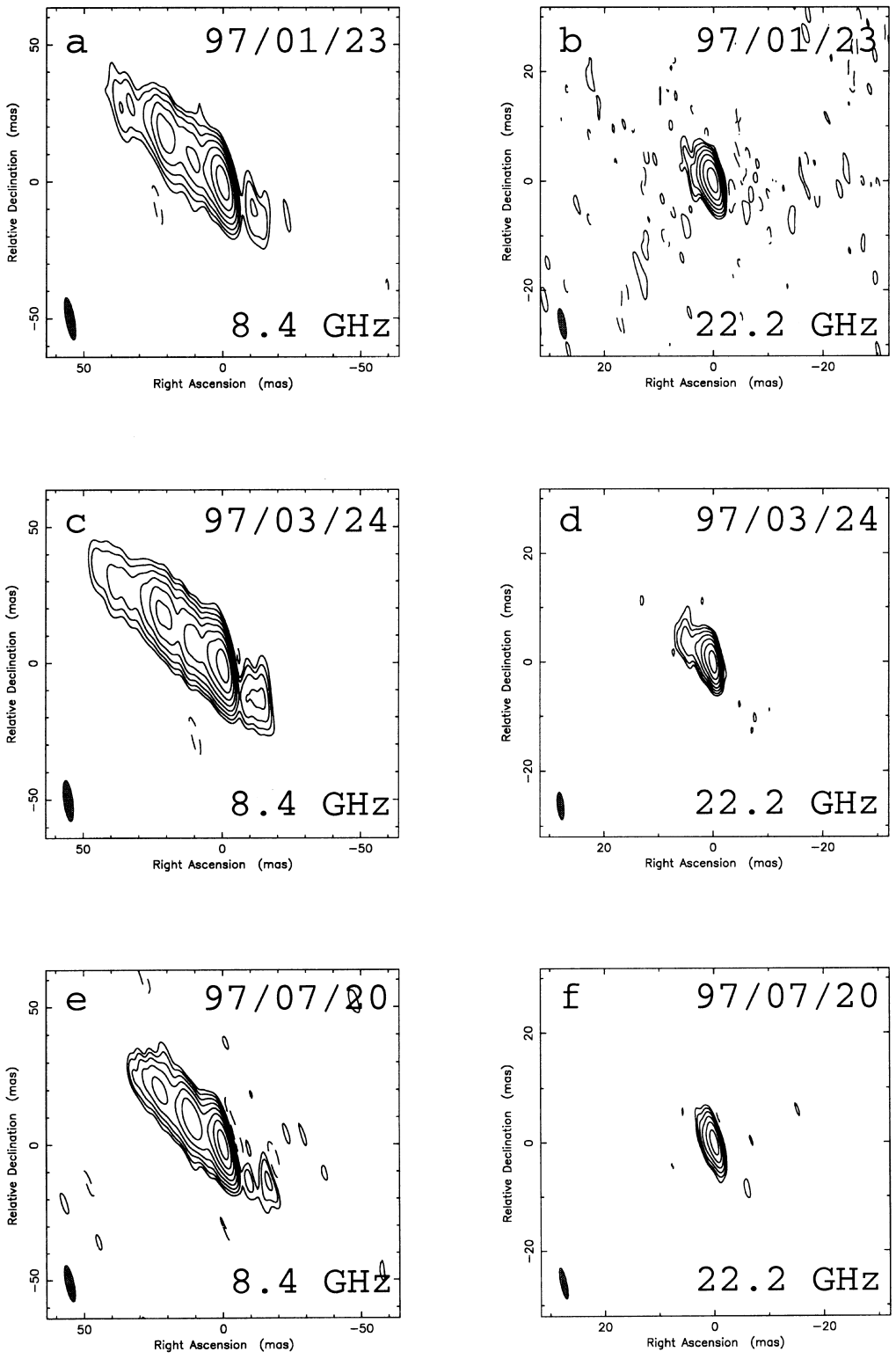

FIG. 1.—Contour levels for (*a*), (*b*), (*d*), (*g*), and (*j*) are − 1%, 1%, 2%, 4%, 8%, 16%, 32%, and 64% of the peak flux density in the map, as given in Table 1. The contour levels for (*f*) are − 2%, 2%, 4%, 8%, 16%, 32%, and 64% of the peak flux density, as given in Table 1. The contour levels for (*c*), (*e*), (*i*), and (*k*) are − 0.5%, 0.5%, 1%, 2%, 4%, 8%, 16%, 32%, and 64% of the peak flux densities, as given in Table 1. The contour levels for (*h*) are − 0.25%, 0.25%, 0.5%, 1%, 2%, 4%, 8%, 16%, 32%, and 64% of the peak flux density, as given in Table 1.

tion of time. Also shown are the flux densities of the same components as a function of time. From the data of T98, the estimated speed for component C3, closest to the core, was consistent with both no motion and the significant motions of components C1 and C2, $\beta_{\mathrm{app-C1}} = 0.13 \pm 0.03$ and $\beta_{\mathrm{app-C2}} = 0.11^{+0.03}_{-0.01}$, respectively (where β_{app} is the apparent component speed in units of the speed of light). The estimated apparent motion of C3 was $\beta_{\mathrm{app-C3}} = 0.04 \pm 0.1$ from T98.

With the addition of the 1997–2000 data, it is now clear that the apparent motion of component C3 is not consistent with the faster apparent motions of components C1 and C2.

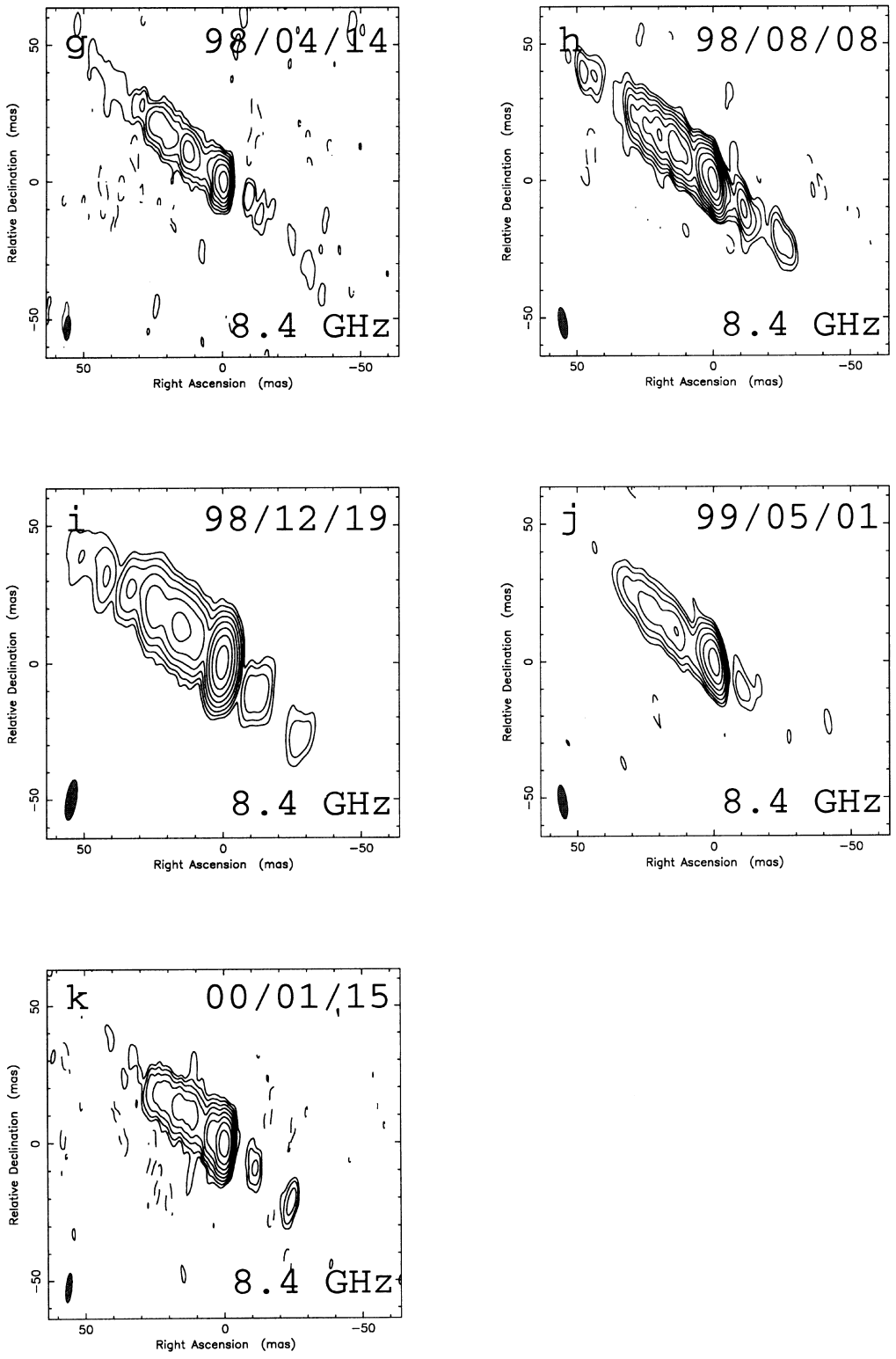

FIG. 1.—*Continued*

Taking the full series of 8.4 GHz data shown in Figure 3, revised estimates of the apparent component motions for C1, C2, and C3 are $\beta_{\mathrm{app-C1}} = 0.12 \pm {}^{0.04}_{0.01}$, $\beta_{\mathrm{app-C2}} = 0.12 \pm {}^{0.02}_{0.03}$, and $\beta_{\mathrm{app-C3}} = 0.01 \pm {}^{0.03}_{0.04}$, respectively. The full series of data clearly show that components C1 and C2 have identical apparent speeds, within the errors, while component C3 appears substantially slower or stationary. The component motions are linear; if the (x, y)-positions of the components are plotted as a function of time, they lie along the 51° position angle of the jet, to within the errors. No significantly curved trajectories are found.

The revised apparent motion estimates are plotted on the montage of images in Figure 2 to show the positional changes of components C1, C2, and C3. At the epoch 1998 August 8, no clear identification of C1 was possible, and these data have been excluded from the least-squares fit for

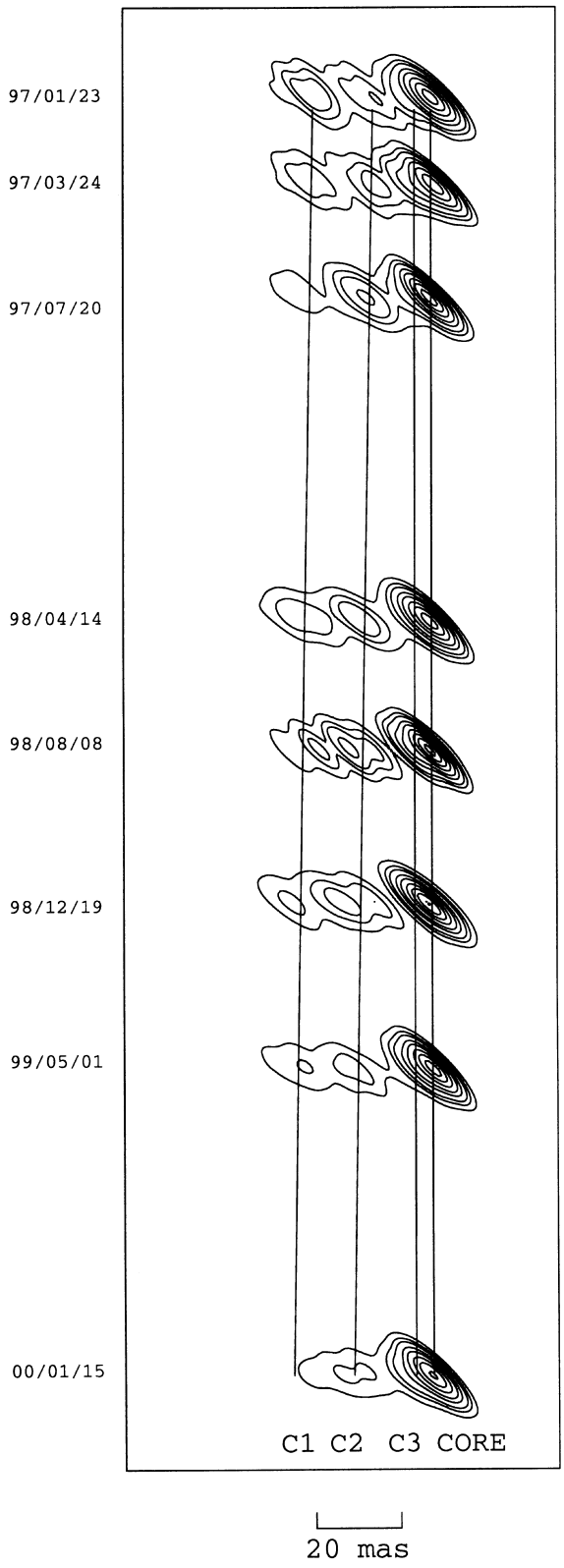

FIG. 2.—Montage showing the series of clean component models from the 8.4 GHz VLBA images. An average restoring beam of 3 × 13 mas at a position angle of 5° has been used. All models and beams have been rotated by 39°. The solid lines are linear least-squares fits to the model-fitted component positions as a function of time.

this component on this basis. Cases similar to this were noted by T98 during the periods of rapid variability in C1 between 1991 and 1993.

With the possibility that C3 is a persistent stationary

TABLE 2

BEST-FIT MODELS FOR THE 8.4 GHz DATA

S (Jy) (1)	d (mas) (2)	θ (deg) (3)	A (mas) (4)	B/A (5)	ϕ (deg) (6)	ID (7)
			1997 Jan 23			
1.82...	0.00	0.0	5.52	0.34	26.6	Core
0.32...	3.32	71.5	3.28	0.00	9.9	C3
0.92...	12.13	51.3	16.40	0.29	37.7	C2
0.65...	26.11	52.0	7.13	0.37	51.5	C1
			1997 Mar 24			
2.28...	0.00	0.0	5.53	0.40	30.1	Core
0.50...	5.66	52.5	5.35	0.00	6.2	C3
0.90...	13.58	49.1	10.25	0.44	23.7	C2
0.76...	26.82	50.6	9.99	0.43	41.9	C1
			1997 Jul 20			
2.33...	0.00	0.0	4.23	0.41	34.4	Core
0.29...	4.87	68.3	7.51	0.00	7.8	C3
1.11...	14.59	49.9	7.87	0.44	32.9	C2
0.53...	28.89	49.6	11.53	0.00	50.3	C1
			1998 Apr 14			
2.48...	0.00	0.0	4.25	0.37	39.2	Core
0.46...	5.18	56.3	8.49	0.32	14.5	C3
1.00...	15.81	49.6	7.45	0.41	36.2	C2
0.93...	28.50	50.4	11.47	0.34	45.1	C1
			1998 Aug 8			
2.40...	0.00	0.0	3.18	0.41	42.6	Core
0.47...	4.27	48.1	6.55	0.00	−4.8	C3
0.33...	17.80	47.8	4.67	0.05	24.4	C2
2.04...	21.00	49.4	22.88	0.03	53.7	C1, C2?
0.13...	14.80	−132.5	6.50	0.29	31.0	CJ2
0.08...	36.81	−133.7	5.60	0.56	47.3	CJ1
			1998 Dec 19			
2.14...	0.00	0.0	3.18	0.69	51.5	Core
0.93...	4.47	23.4	9.82	0.20	35.2	C3
0.85...	17.92	47.3	8.15	0.00	54.6	C2
1.16...	29.89	48.9	17.76	0.31	52.5	C1
			1999 May 1			
2.51...	0.00	0.0	4.00	0.48	36.1	Core
0.48...	5.28	53.5	5.79	0.30	3.7	C3
0.44...	17.68	49.7	7.43	0.00	53.5	C2
1.20...	28.93	50.8	21.45	0.10	52.3	C1
0.07...	11.56	−124.4	14.14	0.00	7.7	CJ2
			2000 Jan 15			
2.00...	0.00	0.00	4.18	0.49	9.8	Core
0.81...	3.72	56.1	4.05	0.76	−11.1	C3
1.32...	17.68	51.2	20.23	0.15	55.7	C2
0.03...	31.66	51.8	23.69	0.00	−23.4	C1
0.04...	16.67	−138.4	5.34	0.00	5.1	CJ2
0.05...	32.82	−132.9	14.61	0.00	−13.0	CJ1

NOTES.—Col. (1): the integrated flux density of the model component in janskys; col. (2): the distance of the model component from the designated phase center in milliarcseconds; col. (3): the position angle of the model component centroid from the designated phase center in degrees east of north; col. (4): the major-axis extent (FWHM) of the model component in milliarcseconds; col. (5): the ratio of model component minor axis to major-axis extent; col. (6): the position angle of the model component major axis in degrees east of north; col. (7): the component identification.

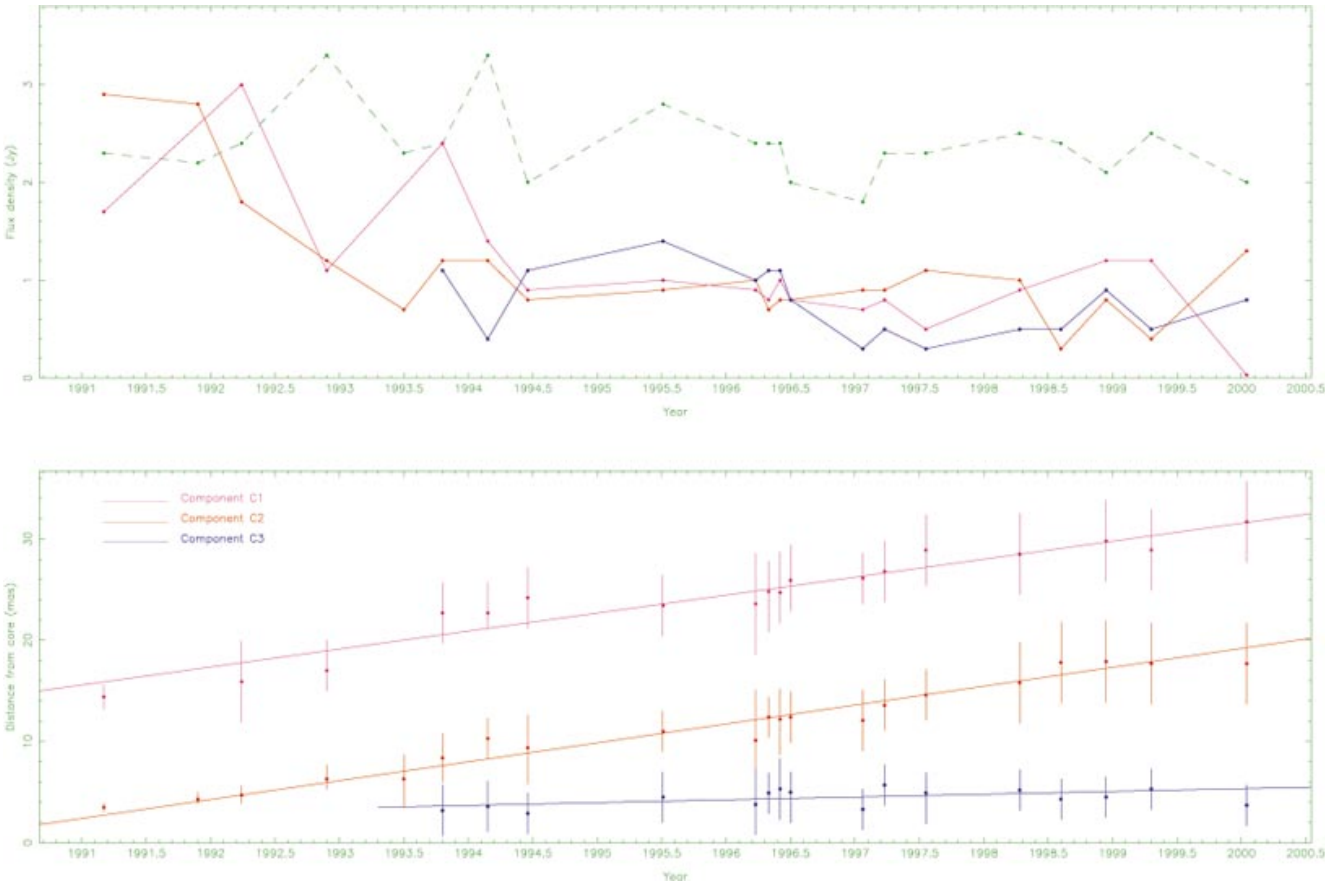

FIG. 3.—Component flux densities (core, C1, C2, and C3) as a function of time (*top*; core flux density is the dashed green line) and the component distances from the core as a function of time (*bottom*). The solid lines in the bottom panel are linear least-squares fits to the data.

component comes the further suggestion that early in the monitoring period, 1991–1993, the components C2 and C3 could not be distinguished and were model-fit as a single component and assigned the label C2. This may explain why C2 initially had a flux density of almost 3 Jy but by mid-1993, when C2 and C3 were first separated, it dropped to the level that it maintained throughout the remainder of the monitoring period, close to 1 Jy. To properly track the flux density variations of C2, we need to subtract the (unknown) flux density of C3 from C2 before mid-1993. Between mid-1993 and mid-1996, C3 had a flux density close to 1 Jy. If this is taken to be indicative of its pre-1993 value, then it would appear that C2 had halved its flux density between ejection from the nucleus and the time at which it could first be distinguished from C3.

T98 noted the dramatic variability in both the structure and flux density of component C1 over a 4 month period late in 1991 and early in 1992 and during another episode in mid-1993. After this time, the monitoring of the subparsec-scale jet of Centaurus A covered in T98 shows no further evidence for high-amplitude, rapid variability of the flux density or structure of any of the jet components. The new data from the 1997–2000 period show that the jet mostly continues in this quiescent state. The core component maintains a flux density of approximately 2 Jy, whereas the components C1, C2, and C3 have maintained reasonably steady flux densities between 0.2 and 1.2 Jy, with evidence for variability on several month timescales but at a much lower level than noted in 1991–1992. Exceptions to this trend are the appearance of C1 at 1998 August 8 noted above and the apparent rapid decline in the flux density of C1 seen in the last of the current series of images at 2000 January 15. Further VLBI monitoring will be required to confirm a change in the state of C1.

Evidence for the short timescale variability of the compact structure in Centaurus A also comes from flux density monitoring at the Australia Telescope Compact Array (ATCA). Figure 4 shows the 8.640 GHz flux density of Centaurus A as seen on the maximum baseline (6 km corresponds to 1″) of the ATCA over a similar period to our VLBA observations. The errors on these points are due to

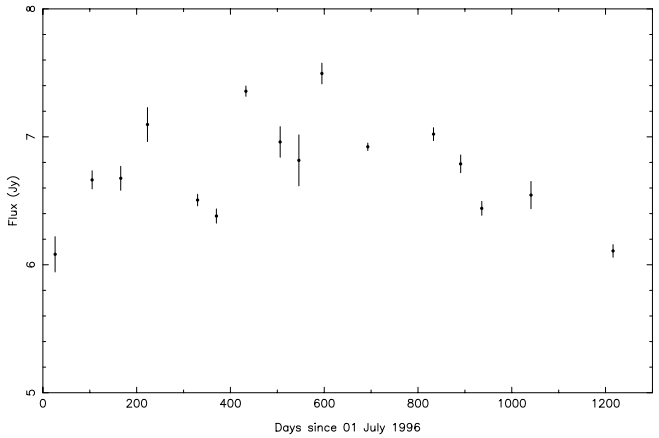

FIG. 4.—ATCA 8.640 GHz flux density monitoring data on the 6 km baseline, corresponding to a 1″ resolution.

nonnuclear (extended jet) emission picked up by the 1″ synthesized beam. The ATCA data show that there is significant flux density missing between the milliarcsecond-scale and arcsecond-scale structures but that the variability seen in the ATCA data corresponds to the typical variations seen with the VLBA, approximately 1 Jy on timescales of a few months.

A feature of the 8.4 GHz images in Figure 1 is the presence of the counterjet, first detected by Jones et al. (1996). Although clearly detected, one must be wary of the details of these counterjet features. Tingay & Murphy (2001) performed simulations to determine the on-source errors due to nonuniqueness in deconvolution for VLBA images of Centaurus A at various frequencies. At 8.4 GHz, they find that for the bright regions of the jet, containing the core and components C1, C2, and C3, the on-source amplitude errors, which are the true limit to dynamic range for sparse arrays, were limited to less than 10%. However, for extended weak jet and counterjet emission, the errors increased to more than 50%. These errors also affect the measured positions of weak features by a significant fraction of a beam.

With this in mind, it is still worth examining the components in the counterjet to determine if they possess any significant apparent motions over the almost 10 yr monitoring period. Figure 5 shows the distance between the counterjet components and the core as a function of time, using the centroids of the counterjet components as measured from the images. Errors on the data in Figure 5 are given by plus and minus the beam size minor-axis FWHM at each individual epoch as an estimate of the maximum error likely to be incurred because of deconvolution errors. The counterjet components are generally too weak to be consistently constrained by model fitting, although at some epochs they are strong enough to affect the model and have been included on these occasions (Table 2).

Linear least-squares fits to the counterjet component distances as a function of time give apparent speeds relative to the core of $\beta_{\mathrm{app-CJ1}} = 0.09 \pm {}^{0.05}_{0.02}$ and $\beta_{\mathrm{app-CJ2}} = 0.04 \pm {}^{0.06}_{0.04}$, where CJ1 is the counterjet component furthest from the core and CJ2 is the counterjet component closer to the core. These apparent motions are away from the core, in the direction opposite to the motion of C1 and C2. The fact that CJ2 is detected far more often than CJ1 shows how close to the detection level these components are; these estimates can only be taken as tentative evidence that the counterjet components have a significant apparent motion. Confirming observations will be required using the more robust combination of the VLBA and SHEVE antennas over a number of years.

3.2. *22 GHz Data*

The 22.2 GHz images shown in Figures 1*b*, 1*d*, and 1*f*, together with the 22.2 GHz image of T98 from 1995 November represent the first multiepoch series of observations of Centaurus A at this frequency. VLBI observations of Centaurus A at 22 GHz and higher frequencies have great potential advantages: angular resolution increases, allowing a higher spatial resolution probe of the jet, and at higher frequencies, the flux density of the nuclear component increases, since the nucleus is both free-free and synchrotron self-absorbed (Tingay & Murphy 2001).

However, Centaurus A is unfortunately placed in the sky, at $\delta \sim -44°$, for high frequency observations with the VLBA. The source is always at low elevations, where atmospheric effects at 22 GHz can be severe. As a result, the 22

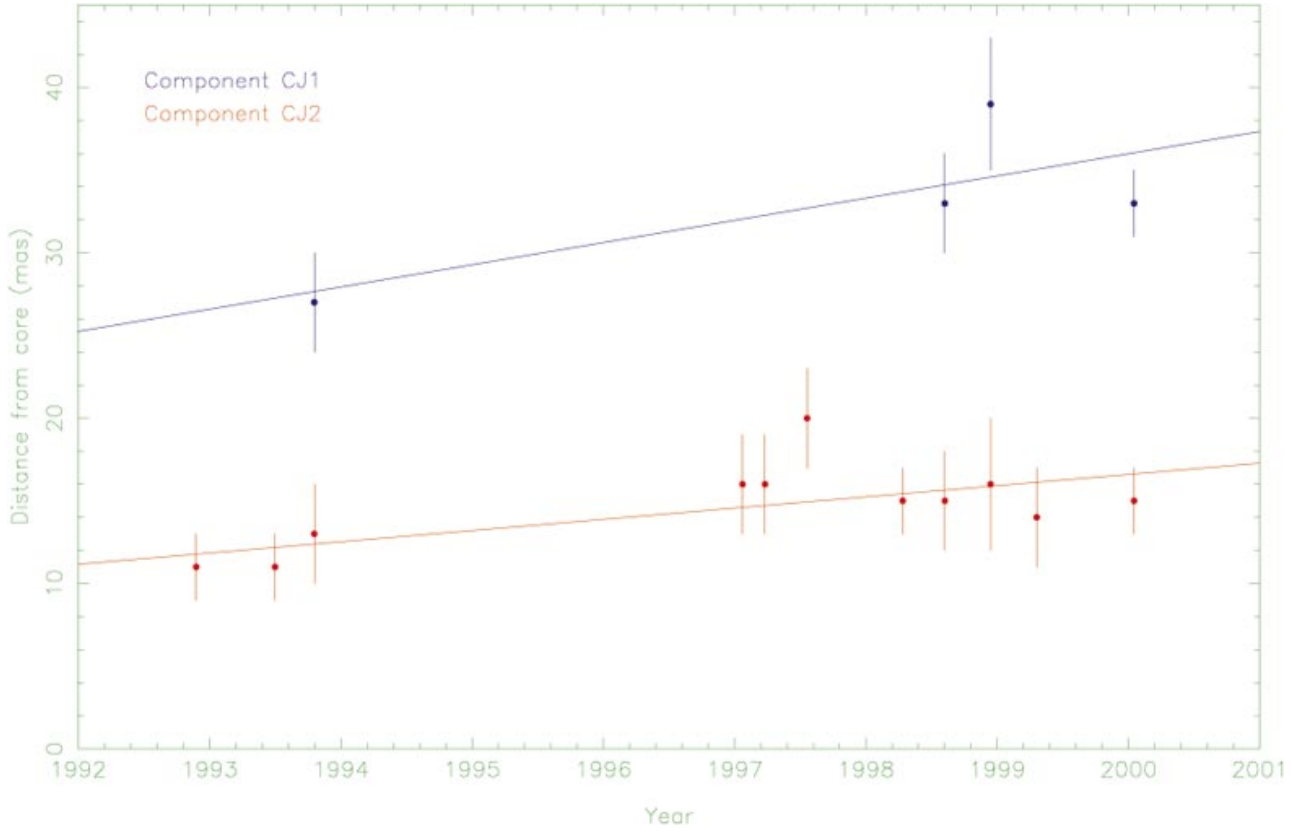

FIG. 5.—Counterjet component distances from the core as a function of time. The solid lines are linear least-squares fits to the data.

TABLE 3

BEST-FIT MODELS FOR THE 22.2 GHz DATA

S (Jy) (1)	d (mas) (2)	θ (deg) (3)	A (mas) (4)	B/A (5)	ϕ (deg) (6)
		1995 Nov 17			
2.50.....	0.00	0.0	1.04	0.07	62.9
0.72.....	0.91	63.2	1.52	0.38	77.0
0.69.....	2.30	49.3	2.92	0.63	−72.6
0.18.....	7.26	42.0	2.17	0.00	−56.0
		1997 Mar 24			
2.20.....	0.00	0.0	1.38	0.35	32.1
0.69.....	1.60	54.4	1.11	0.59	60.0
0.09.....	3.11	56.1	2.88	0.00	−3.6
0.36.....	6.30	48.2	4.96	0.47	24.6

NOTES.—Columns are the same as for Table 2, but without column (7).

GHz images presented here vary substantially in quality, in direct relation to the conditions during the individual experiments.

Only the nuclear component is detected in all four data sets, along with components that correspond to C3. C1 and C2 both have steep spectra and are extended, therefore are difficult to detect at 22 GHz even in good conditions. The best images (the 1995 November image of T98 and the image of 1997 March in Fig. 1*d*) show a similar structure; the nucleus and a jet, slightly extended in the direction seen in the lower frequency images. These two data sets have been model-fit, as described above, and the results are shown in Table 3. The 22.2 GHz model fits show that the jet structure is highly linear close to the nucleus; the average position angle of the fitted components in Table 3, within 10 mas of the core, is 52°.2, with an rms deviation of only 6°.7 around that average. This compares to the position angle of the jet on larger scales and at lower frequencies of 51°. We hesitate to directly identify any of the individual components in the 22 GHz models of Table 3 with the component identified as C3 in Table 2. Given that the 22 GHz data suffer from the problems described in § 2 and the fact that the C3 region appears to be complicated at 22 GHz, we would have little confidence in an absolute identification of components based solely on two reasonable observations. At the moment, the 22 GHz data only allow us to conclude that emission from a region coincident with C3 is apparent, which can be modeled as a linear structure, consistent with what is seen at 8.4 GHz.

Further VLBI observations from the Southern Hemisphere at 22 GHz, which would be less affected by atmospheric opacity, will be required to probe the detailed structure of the C3 component.

4. DISCUSSION AND CONCLUSIONS

4.1. *What is the Nature of C3?*

The component C3 appears to be stationary, or at least very slowly moving, approximately 4 mas from the core component, which corresponds to approximately 0.3 lt-yr in projected distance. This is in contrast to components C1 and C2, which have moved gradually away from the core with an average apparent speed of 0.12c over an almost 10 yr period.

Stationary components in parsec- and subparsec-scale jets are not uncommon and are sometimes ascribed to the effects of relativistic beaming at a point in the jet where the jet bends toward the line of sight, producing amplified emission from the region at the bend that is most aligned with our line of sight. However, these effects are most likely to be seen in jets in core-dominated radio sources, those jets that are already highly aligned with our line of sight, since then a small bend can produce a dramatic effect. In a jet such as in Centaurus A, estimated to lie between 50° and 80° to our line of sight, a small bend will not have a dramatic effect and a very large intrinsic bend would be required, which is unlikely, while retaining jet collimation.

Interestingly, Fujisawa et al. (2000) claim to have found a large jet bend close to the position of component C3 from intercontinental VLBI observations at 5 GHz as part of a VLBI Space Observatory Programme observation. Of four observations, only one provided data good enough to image, and Centaurus A was not detected on the space baselines during any observation. From these data, Fujisawa et al. (2000) claim an intrinsic jet bend of greater than 52°, a distance 3 mas from the Centaurus A core, close to the model-fit position of C3. Fujisawa et al. (2000) cite further evidence of the jet bend from the 1995 November 22.2 GHz image of T98, which they suggest shows the same bend as their 5 GHz data. We have quantified the 22.2 GHz structure of the Centaurus A jet in § 3.2 above by model-fitting the 1995 November and 1997 March data. Overall, in both cases the jet within 10 mas of the core is linear in structure and can be parameterized by a small number of components sharing the same position angle as observed at lower frequencies.

We suggest that the 1995 November 22.2 GHz image of T98 might appear to suggest a bend near the core by virtue of the size and shape of the restoring beam. Given that our 22.2 GHz data do not show evidence for a bend, we also suggest that the 5 GHz image of Fujisawa et al. (2000) should be interpreted with caution. In particular, the u-v coverage of the observation is very sparse, and the image appears to be affected by on-source errors, as described in § 3.1. An analysis of on-source errors, similar to that described in Tingay & Murphy (2001) or Lister et al. (2001), would help greatly in determining if the structure in the image of Fujisawa et al. (2000) is likely to be real.

In the following, we base our interpretation of C3 on the data presented here, which show a stationary, or slowly moving, linear extension to the core. The component C3 seems to be typical of a type of feature that has been seen in several different sources that have been imaged at very high spatial resolution. These features manifest themselves as persistent stationary extensions to the core. A situation exactly analogous to that seen in Centaurus A has been noted in the galactic superluminal source GRO J1655−40 (Tingay et al. 1995; Hjellming & Rupen 1995). GRO J1655−40 produced superluminal jet components at an angle to our line of sight of 84°. In addition to the rapidly moving jet components, a stationary extension to the core was found (Tingay et al. 1995). In addition, in 3C 120 Gómez et al. (2000) note the existence of a stationary component 0.8 mas, or approximately 2 pc, in projected distance from the core. In this case, the jet is estimated to lie within approximately 20° of our line of sight.

Agudo et al. (2001) have developed numerical simulations that describe the response of an expanding relativistic jet to

strong perturbations at the jet origin. These simulations show that a single strong perturbation can produce a major component in the jet and a series of trailing components, which should appear in VLBI images, also in motion away from the core. The trailing components travel slower than the component produced by the original perturbation, although they have speeds that are a function of distance along the jet. Close to the core the trailing components appear to be almost stationary, whereas further from the core, the trailing components may have speeds close to the speed of the original perturbation. Agudo et al. (2001) cite the stationary component in the parsec-scale jet of 3C 120 as a possible example of a quasi-stationary component trailing the main perturbation.

These simulations offer an attractive explanation for the behavior of component C3, since C3 appears to be stationary close to the core, and trailing components C1 and C2, presumably the products of major perturbations. In fact, the simulations of Agudo et al. (2001) may also neatly explain another aspect of the subparsec-scale jet in Centaurus A, the sometimes dramatic internal variability of components that does not appear to affect their long-term apparent speeds. These variations could occur when a new major perturbation in the jet overtakes the trailing shocks of a previous major perturbation, such as observed in 3C 120 (Gómez et al. 2000).

In this case, as the major perturbation traverses the slower trailing shocks, interaction between the two shocks could cause enhanced synchrotron emission. Evidence for this was seen in 3C 120. When a major perturbation crossed the stationary component close to the core, the polarization of both components increased, indicating an increase in the ordering of the magnetic field at that point. Polarization VLBI will be extremely valuable in investigating this possibility for Centaurus A in the future.

4.2. *Constraints on the True Component Speed and Jet Viewing Angle*

If apparent component motions in an approaching jet and the corresponding receding (counter) jet can be measured, then by making the assumption that both approaching and receding components have identical intrinsic speeds and are intrinsically collinear, the true component speed and jet angle to the line of sight can be determined (e.g., as a variation on the equations presented by Taylor & Vermeulen 1997). The expressions that give the intrinsic component speed (β) and jet angle to the line of sight (θ) are

$$\theta = \tan^{-1}\left(\frac{2\beta^a_{\rm app}\beta^r_{\rm app}}{\beta^a_{\rm app} - \beta^r_{\rm app}}\right),$$

$$\beta = \frac{\beta^a_{\rm app}}{\beta^a_{\rm app}\cos\theta + \sin\theta},$$

where $\beta^a_{\rm app}$ and $\beta^r_{\rm app}$ are the apparent speeds of the approaching and receding components, respectively. The likely range in jet angle to the line of sight suggested in T98, 50°–80°, along with our well-measured value of $\beta^a_{\rm app} = 0.12 \pm {}^{0.04}_{0.03}$, imply that $\beta^r_{\rm app}$ should lie in the range 0.08–0.13, which is consistent with the estimated errors on the apparent speeds of CJ1 and CJ2. Over this range, the intrinsic speeds of both the jet and counterjet components would lie in the range $0.09 < \beta < 0.20$.

A precise constraint on the intrinsic component speed and jet angle to the line of sight from the measured apparent motions of counterjet components will require further VLBI monitoring, probably with a combination of the VLBA and SHEVE arrays (to improve the *u-v* coverage and the reliability of the estimated component positions), but appears to be a feasible goal. Such a measurement is very important, for example, to constrain the inclination of the disk of material observed by Marconi et al. (2001), which would in turn constrain the upper limit to the central black hole mass in Centaurus A (Marconi et al. 2001; assuming that the radio jet lies perpendicular to the disk orbiting the black hole).

4.3. *Comparison with M87*

M87 is one of the closest radio galaxies, 14.7 Mpc away, although 4 times more distant than Centaurus A. The high-resolution properties of the most nearby radio galaxies, such as M87 and Centaurus A, could offer some insights into the physical processes that form and collimate relativistic jets.

A comparison of the VLBI properties of Centaurus A and M87 has already been made in T98; however, new VLBI and optical/infrared results for both Centaurus A and M87 prompt us to revisit the comparison. Junor, Biretta, & Livio (1999) have recently imaged the jet of M87 on angular scales down to 0.12 mas with VLBI, corresponding to a spatial scale of 0.009 pc, or 30 Schwarzschild radii (for the estimated M87 black hole mass of $3 \times 10^9\ M_\odot$). They show that the M87 jet on these scales has a remarkably large opening angle of $\sim 60°$, which decreases strongly with distance from the core.

An estimate of the central black hole mass for Centaurus A has recently been made using the VLT, $2 \pm {}^{3.0}_{1.4} \times 10^8\ M_\odot$ (Marconi et al. 2001), approximately an order of magnitude less than for M87. Thus, from the highest resolution images of Figure 1, the smallest spatial scale we probe in Centaurus A is approximately 0.02 pc, corresponding to $1000 \pm {}^{2000}_{600}$ Schwarzschild radii.

Based on their data, Junor et al. (1999) suggest that the collimation of the M87 jet first occurs on scales corresponding to ~ 100 Schwarzschild radii and continues out to 1000 Schwarzschild radii. We have examined our 8.4 and 22.2 GHz data to see if we could measure a jet opening angle on scales greater than 1000 Schwarzschild radii, which would indicate how collimated the jet is on these scales. Figure 6 shows the projected width of the jet as a function of project-

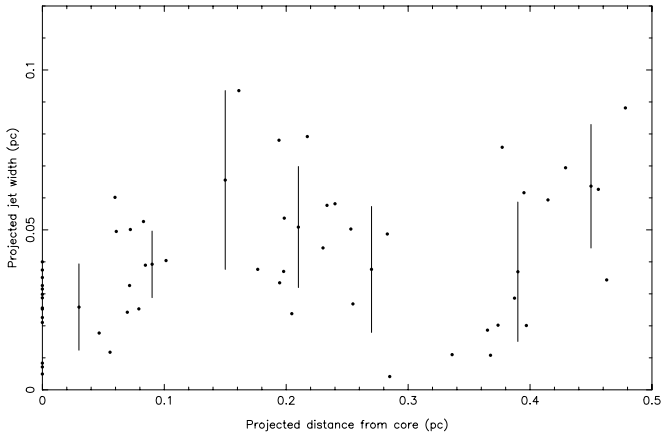

FIG. 6.—Projected jet width as a function of projected distance away from the jet (not including the counterjet) for the full series of 8.4 GHz observations.

ed distance along the jet for the 8.4 GHz data. Each point in Figure 6 represents the extent of one model component in the direction perpendicular to the jet direction; model components from all our 8.4 GHz model fits have been used. The points with error bars are the average widths over 0.03 pc bins, the error bars being the rms around the average. No evidence for a significant jet opening angle can be seen in these data. The 22 GHz data are not shown because far fewer model components are available. However, the 22 GHz data are consistent with the 8.4 GHz data, no evidence for a jet opening angle could be found.

It appears likely that the initial region of collimation in Centaurus A occurs on a scale similar to that seen in M87. This scale lies well below our resolution limit due simply to the fact that the Centaurus A black hole is an order of magnitude lighter than the M87 black hole, and the angular resolution we can achieve for Centaurus A with the VLBA is limited by its southerly declination. Space VLBI observations at 22 and 43 GHz will probably be required to probe the collimation region in Centaurus A, providing the extra factor of ~ 10 in angular resolution needed to probe below 1000 Schwarzschild radii.

5. SUMMARY

VLBA monitoring of the subparsec-scale jet in Centaurus A has now been undertaken over the period 1992–2000 and has allowed us to

1. confirm that the apparent speeds of two components in the subparsec-scale jet (C1 and C2) are identical to within the errors at $0.12c$;
2. improve our estimate of the apparent speed of another component (C3), which is much closer to the core, and show that it is stationary or significantly slower than the components further away from the core;
3. present the first series of 22 GHz VLBI images of Centaurus A that show that the jet is highly linear and collimated on scales as small as 0.02 pc;
4. tentatively detect the motion of components in the counterjet and show that the estimated jet and counterjet apparent speeds are consistent with our previously suggested range in jet viewing angle, 50°–80°;
5. suggest that the variability of components in the jet, as well as the stationary nature of component C3, may be explained by the processes illustrated by the numerical simulations of Agudo et al. (2001); and
6. determine that the region of initial collimation of the Centaurus A jet likely occurs on angular scales of ~ 100 μas, requiring the resolution of the next generation of space VLBI missions.

Part of this work was undertaken while S. J. T. held a National Research Council–NASA/JPL Research Associateship. Part of this work was carried out at the Jet Propulsion Laboratory, California Institute of Technology, under contract with NASA. The Australia Telescope is funded by the Commonwealth of Australia for operation as a national facility managed by the CSIRO. The Astronomical Image Processing Software and the VLBA were developed and are maintained by the National Radio Astronomy Observatory, which is a facility of the National Science Foundation operated under cooperative agreement by Association Universities, Inc. We thank the anonymous referee for comments that improved the paper.

REFERENCES

Agudo, I., Gómez, J.-L., Martí, J.-M., Ibáñez, J.-M., Marscher, A. P., Alberdi, A., Aloy, M.-A., & Hardee, P. E. 2001, ApJ, 549, L183
Fujisawa, K., et al. 2000, PASJ, 52, 1021
Gómez, J.-L., Marscher, A. P., Alberdi, A., Jorstad, S. G., & García-Miró, C. 2000, Science, 289, 2317
Hjellming, R. M., & Rupen, M. P. 1995, Nature, 375, 464
Israel, F. P. 1998, A&A Rev., 8, 237
Jacoby, G. H., Ciardullo, R., & Ford, H. C. 1990, ApJ, 356, 332
Jones, D. L., et al. 1996, ApJ, 466, L63
Junor, W., Biretta, J. A., & Livio, M. 1999, Nature, 401, 891
Kraft, R. P., et al. 2000, ApJ, 531, L9
Lister, M. L., Tingay, S. J., Murphy, D. W., Piner, B. G., Jones, D. L., & Preston, R. A. 2001, ApJ, 554, 948
Marconi, A., Capetti, A., Axon, D. J., Koekemoer, A., Macchetto, D., & Schreier, E. J. 2001, ApJ, 549, 915
Pearson, T. J. 1991, BAAS, 23, 991
Shepherd, M. C., Pearson, T. J., & Taylor, G. B. 1994, BAAS, 26, 987
Schreier, E. J., et al. 1998, ApJ, 499, L143
Taylor, G. B., & Vermeulen, R. C. 1997, ApJ, 485, L9
Tingay, S. J., et al. 1995, Nature, 374, 141
———. 1998, AJ, 115, 960 (T98)
Tingay, S. J., & Murphy, D. W. 2001, ApJ, 546, 210